J Therm Anal Calorim (2014) 116:1001–1010
DOI 10.1007/s10973-013-3599-9

Analysis of the heat generation of lithium-ion battery during charging and discharging considering different influencing factors

Guangming Liu · Minggao Ouyang · Languang Lu · Jianqiu Li · Xuebing Han

Received: 6 June 2013 / Accepted: 15 December 2013 / Published online: 31 January 2014

Abstract Operating temperature of lithium-ion battery is an important factor influencing the performance of electric vehicles. During charging and discharging process, battery temperature varies due to internal heat generation, calling for analysis of battery heat generation rate. The generated heat consists of Joule heat and reaction heat, and both are affected by various factors, including temperature, battery aging effect, state of charge (SOC), and operation current. In this article, a series of experiments based on a power-type lithium manganese oxide/graphite battery was implemented under different conditions. The parameters for Joule heat and reaction heat are determined, and the Joule heat, reaction heat as well as total heat generation rate is detailed and analyzed considering the influence of temperature, aging, SOC, and current. In order to validate the accuracy of heat generation rate, a lumped battery heat transfer model is applied to calculate the temperature variation, and the estimated temperature variation shows good correspondence with experimental results under different currents and aging conditions. Due to its simplicity, the temperature variation estimation method is suitable for real time applications.

Keywords Lithium-ion battery · Heat generation analysis · Heat generation influencing factors · Temperature variation estimation

G. Liu · M. Ouyang (✉) · L. Lu · J. Li · X. Han
State Key Laboratory of Automotive Safety and Energy, Tsinghua University, Beijing 100084, China
e-mail: ouymg@tsinghua.edu.cn

G. Liu
e-mail: lgm06@mails.tsinghua.edu.cn

Introduction

Comparing with lead-acid batteries and nickel-metal hydride batteries, lithium-ion batteries have higher energy and power density as well as better durability [1], and are consequently widely implemented on electric vehicles (EV). As a complicated electrochemical power source, lithium-ion battery's performance is greatly affected by its operating temperature. When the temperature decreases, the battery's internal resistance increases while the available capacity decreases, leading to the shrinkage of battery available energy and maximum power. As a result, the EV driving range and acceleration performance are strongly affected under low temperature [2, 3]. At high temperature, however, lithium-ion battery suffers from safety and aging problems [4, 5]. The battery temperature varies not only with the environment temperature change, but also due to internal heat generation during charge and discharge [6, 7]. Consequently, the heat generation of lithium-ion battery during charging/discharging process should be analyzed in detail, so as to guarantee the accuracy of battery temperature prediction.

The lithium-ion battery heat generation was mentioned in previous research through thermal–electrochemical modeling [8–10], in which the internal heat generation during regular charge/discharge is presented as Eq. 1. $\dot{Q}$ is the heat generation rate (positive for heat generation and negative for heat absorption), I is the battery operating current (positive for discharging and negative for charging), U_t is the battery terminal voltage, U_{OCV} is the battery open circuit voltage (OCV), T is the battery temperature, ΔH_i is the entropy change of the ith chemical reaction, r_i is the reaction rate of the ith reaction, $\bar{H}_j$ is the molar entropy of the jth piece of the battery (describing the spatial variation in battery cells), c_j is the ion concentration in jth

piece, and v is the volume. The value with superscript "avg" means an average concentration in a certain volume. The first part on the right side indicates the resistive Joule heat (abbreviated as $\dot{Q}_{\text{jou}}$), the second part is the reversible entropic heat or reaction heat (abbreviated as $\dot{Q}_{\text{jou}}$), indicating the entropy change in charge and discharge process. The third part is the heat in side reaction indicating the aging process (abbreviated as $\dot{Q}_{\text{sr}}$), and the fourth part is the heat in mixing process (abbreviated as $\dot{Q}_{\text{mix}}$). The aging process of lithium-ion battery is very slow, meaning very low side-reaction rate in a single charge/discharge cycle [11]. The heat in mixing process is due to the formation and relaxation of cell concentration gradients, which is more important under dynamic charge/discharge profiles and not significant in applications with constant current [12]. In this article, the battery was mainly tested under constant charge/discharge current, so $\dot{Q}_{\text{sr}}$ and $\dot{Q}_{\text{mix}}$ is insignificant comparing with Joule and reaction heat. As a result, the heat generation during charge and discharge can be calculated in Eq. 2.

$$\dot{Q} = I(U_{\text{OCV}} - U_{\text{t}}) - IT\frac{\partial U_{\text{OCV}}}{\partial T} - \sum_{\text{i}} \Delta H_{\text{i}}^{\text{avg}} r_{\text{i}} - \int \sum_{\text{j}} (\bar{H}_{\text{j}} - \bar{H}_{\text{j}}^{\text{avg}}) \frac{\partial c_{\text{j}}}{\partial t} \text{d}v \quad (1)$$

$$\dot{Q} = \dot{Q}_{\text{jou}} + \dot{Q}_{\text{re}} = I(U_{\text{OCV}} - U_{\text{t}}) - IT\frac{\partial U_{\text{OCV}}}{\partial T} \quad (2)$$

As shown in Eq. 2, the Joule heat is determined by the battery operating current and the overpotential, while the overpotential can be explained as the voltage drop on battery internal resistance. As a result, the battery internal resistance R_{in} during charge and discharge can be determined by Eq. 3. The internal resistance of lithium-ion battery is mainly influenced by temperature, state of charge (SOC), and battery aging, and the general influence of these factors is clear: the resistance increases with the decrease of operating temperature and varies in different SOC areas, and there is a continuous growth in battery resistance with the growth of cycle number [13, 14]. But, the detailed impact of temperature, SOC, and aging on internal resistance for different lithium-ion batteries varies largely due to variation in cell chemistry and production process, and specific experiments are needed for the Li-ion battery in our research.

$$R_{\text{in}} = \frac{U_{\text{OCV}} - U_{\text{t}}}{I} \quad (3)$$

The reaction heat is determined by the battery operating current and the effective entropic potential ($T\partial U_{\text{OCV}}/\partial T$, written as $T\partial U_{\text{OCV}}/\text{d}T$ for convenience, in which T stands for absolute temperature). The entropic potential is strongly influenced by battery SOC, and it varies significantly with different chemistry [15]. The influence of temperature on entropic potential is still not clear, since the entropic potential was usually calibrated under a narrow temperature range [11, 16], the entropic potential calibration on the hole operating temperature range (−20 to 55 °C for an automotive-oriented lithium-ion battery) was seldom performed. Moreover, few of the previous study discussed the influence of battery aging on effective entropic potential. Therefore, more experiments are needed to determine the impact of SOC, temperature and battery aging on entropic potential.

Based on a type of lithium-ion battery, this study investigates the heat generation parameters for Joule and reaction heat generation through a set of experiments, and discusses the quantitative influence of different factors (operating current, SOC, temperature, and battery aging) on the heat generating rate during charging and discharging process. The contribution ratio of Joule and reaction heat on the total heat generation is also analyzed considering different influencing factors. The heat generation analysis is then applied along with a lumped heat transfer model to calculate the temperature variation during discharge, and the result corresponds well with experiment.

Identification of heat generation parameters considering different influencing factors

As shown in Eqs. 2 and 3, the Joule heat is determined by the operating current and internal resistance, and the reaction heat is determined by the current and entropic potential. In order to calculate the heat generation precisely, the influence of SOC, battery aging, and temperature on battery heat generation parameters (internal resistance for Joule heat, and entropic potential for reaction heat) needs to be attentively calibrated.

Among Li-ion batteries with different electrode materials, lithium manganese oxide/graphite battery (LMO-G) owns better abuse tolerance comparing with the lithium cobalt oxide/graphite and the Li–nickel–cobalt–aluminum/graphite, and its energy density is much higher than the lithium iron phosphate/graphite and batteries with lithium titanium oxide anode [17]. As a result, the LMO-G battery is one of the most frequently used lithium ion battery in automotive industry. In this article, we use a power type prismatic LMO-G with nominal capacity 8 Ah. The battery has a maximum discharge current rate of 20C (160 A) and maximum charge current rate of 10C (80 A), and the operating temperature range is from −20 to 55 °C. A BTS-3000 battery testing instrument produced by Neware Corporation is implemented to charge and discharge the battery with voltage range 0–5 V and current range −200 to 200 A. A TEMI880 temperature chamber produced by Puhua Corporation is used to limit the temperature

fluctuation for most of the tests, including battery capacity calibration, internal resistance calibration (i.e., HPPC test), entropic potential calibration, and the charge/discharge experiments in "Experimental validation of heat generation analysis through temperature variation calculation" section. The chamber can keep the temperature constant at a set value between −40 and 150 °C, and the temperature variation is within ±0.5 °C. The chamber is equipped with a nichrome heating wire for heating, a hermetic compressor for cooling, and a low-speed centrifugal fan to control the chamber air movement. Consequently, a weak forced convection environment is provided for the test cell. During the battery aging process, however, the temperature chamber was thought not capable to keep the cell temperature under 55 °C, since the battery experienced 20C discharge current and could generate a lot of heat. A specific cooling module was here implemented, in which a cooling fan was placed directly against the cell to provide a strong forced convection condition. During aging process, the battery temperature was kept under 50 °C. The cell temperature was measured using AD 590 temperature sensor integrated on the Neware battery testing system, and the measuring accuracy is ±0.3 °C, with temperature range −40 to 150 °C. The battery testing system has a 14-bit AD module, meaning the temperature resolution is 0.016 °C. One temperature sensor was placed at the front surface center of each cell.

Identification of internal resistance variation under different operating conditions

The battery internal resistance varies under different temperatures, SOCs and aging conditions, leading to the variation of Joule heat generation under the same operating current. In order to determine the aging effect on Joule heat generation, two cells in the same production batch were used to compare the performance variation before and after aging process. We designed an aggressive charge/discharge cycle in order to accelerate battery aging, with a three-phase charging process with current rate 4C (32 A), 1C (8 A), and 0.1C (0.8 A), all the three phase with a voltage upper limit of 4.2 V, and a discharging process with 20C (160 A) discharge, with a voltage lower limit of 3.0 V. The discharge current (20C) is the maximum allowed discharge current according to the battery handbook, and the three-phase constant current charge was chosen to minimize charging time as well as ensure the battery safety, since high-rate charge at high SOC may lead to battery failure. Ten-minute rest was taken after each charge/discharge process to lower the battery temperature. One cell was charged and discharged for 300 cycles in 3 weeks, and the other cell was taken as reference (stored at room temperature). The two cells are considered as the "aged cell" and "new cell" in the following parts.

In order to precisely calibrate the influence of temperature, SOC as well as aging effect, the battery was systematically tested under standard testing cycle. Capacity test was implemented for both the new and aged cell. Under 25 °C, 1C current (8 A according to nominal capacity 8 Ah), the discharge capacities of the new and aged cells are, respectively, 8.727 and 8.029 Ah. Battery state of health (SOH) could be defined as the ratio of cell current capacity and initial capacity [5]. As a result, the aged cell has 92 % SOH, meaning 8 % capacity loss after the aging process. The Hybrid Pulse Power Characterization (HPPC) test is designed to determine the internal resistance at different SOC points for power-type battery in hybrid EV application [18], and was employed for both the aged and the new cell under different temperatures (5, 25 and 45 °C). In HPPC test, the cell was first discharged and fully charged under standard conditions (1C, 25 °C), and then adjusted to different SOC value to calibrate the internal resistance by pulse current under test temperature (5, 25 or 45 °C). Cell SOC was calculated according to the real capacity (8.029 Ah for the aged cell and 8.727 Ah for the new one). The pulse discharge current for resistance calibration was 10C (80 A), and the pulse charge current was 7.5C (60 A). The test result for discharge resistance is shown in Fig. 1a. The internal resistance increases with decreased temperature and battery aging, and the temperature influence is more significant than cell degradation, which is in accordance with the results in [19]. The discharge resistance is relatively constant at SOC above 50 %, and increases with decreased SOC at low-SOC range. It can be inferred that at high-SOC range, the importance of Joule-heat influencing factors is ranked as temperature, aging effect and SOC, while at low-SOC range, the SOC value is most crucial, followed by temperature and aging effect. Figure 1b provides the result of charge resistance. It is obvious that charge resistance is smaller than discharge resistance, meaning a smaller Joule heat production in charging process. And cell degradation results in larger charge resistance growth than discharge resistance, meaning that aging effect is more crucial in Joule heat calculation during charging.

Identification of reaction heat generation parameters considering different influencing factors

According to [8], there are two experimental methods to measure the reaction heat. The first method is based on calorimetry. It is assumed that upon charge and discharge, Joule heat remains constant while reaction heat is opposite. Through accelerated-rate calorimetry or isothermal heat conduction calorimetry, charge calorimeter data are subtracted by the discharge calorimeter data to calculate the reaction heat. But, the resistances during charge and

discharge are usually not identical (the resistance in Fig. 1, e.g.), leading to difference in Joule heat generation, and the battery's large heat capacity results in inaccuracy of heat generation measurement. The second method is based on Eq. 2, and calculates the effective entropic potential (TdU_{OCV}/dT) by measuring the OCV variation under different temperatures. This method is widely used and the calculated $\dot{Q}_{re}$ corresponds well with the experimental result [11, 16, 20], hence it was implemented in our study.

In former studies, however, the testing temperature range was narrow (6–26 °C in [11] and 21–29 °C in [16], e.g.), and few of the studies considered the aging effect. In this article, however, the influences of battery aging and SOC on entropic potential are investigated in the entire operating temperature range (−20 to 55 °C). Nine SOC points were equally spaced in SOC range 0–100 %. For each SOC point, temperature was adjusted in a fixed cycle (25, 55, 25, 0, −20, and 25 °C). The waiting time was 3 h for the temperatures above 0 °C and 5 h for 0 and −20 °C. An example of voltage variation within the temperature cycle is provided in Fig. 2 (aged cell, SOC adjusted at 75 %). Except for the voltage change due to temperature variation, a voltage decrease is observed in waiting process owning to battery self-discharge, especially at high temperature. In order to minimize the influence of self-discharge, the voltage variation during temperature change is compensated by calculating the voltage drop gradient in the previous temperature point, as explained in [16]. The entropic heat coefficient (dU_{OCV}/dT) was calculated based on the OCV at different SOC and temperature. By multiplying entropic heat coefficient and absolute temperature T, a 2-D entropic potential lookup table considering SOC and temperature was derived.

Figure 3a, b shows the entropic potential (with a unit "mV", written as U_{ep} for simplicity) for the new cell and the aged cell. It is obvious that the influence of SOC is much larger than the temperature influence on the entropic potential variation. In order to determine the influence of battery aging more clearly, a two-dimension figure considering entropic potential under different SOC and aging conditions at fixed temperature (25 °C) is provided in Fig. 4a. U_{ep} varies significantly with SOC, and cell degradation has large influence on the entropic heat around 75 % SOC, while the impact is little in other SOC range. The aging-based entropic potential change is probably caused by the loss of active electrode material during degradation, as explained by incremental capacity analysis in [21]. The temperature influence is less significant than SOC for U_{ep} calculation, but the U_{ep} difference with large temperature gap is also assignable (the U_{ep} at 0 % SOC under 55 and −20 °C are, respectively, −102 and −80 mV, with 25 % difference, e.g.). Conclusively, battery SOC is the most important issue influencing reaction heat generation, aging effect should also be considered in some SOC points, while the influence of temperature is not negligible. In the following analysis, the entropic potential considering SOC, temperature and aging influence (i.e., the results in Fig. 3a, b) is implemented. It is also noticed that the entropic change (ΔS) of a LMO-G cell was calibrated in previous researches [15], and the corresponded

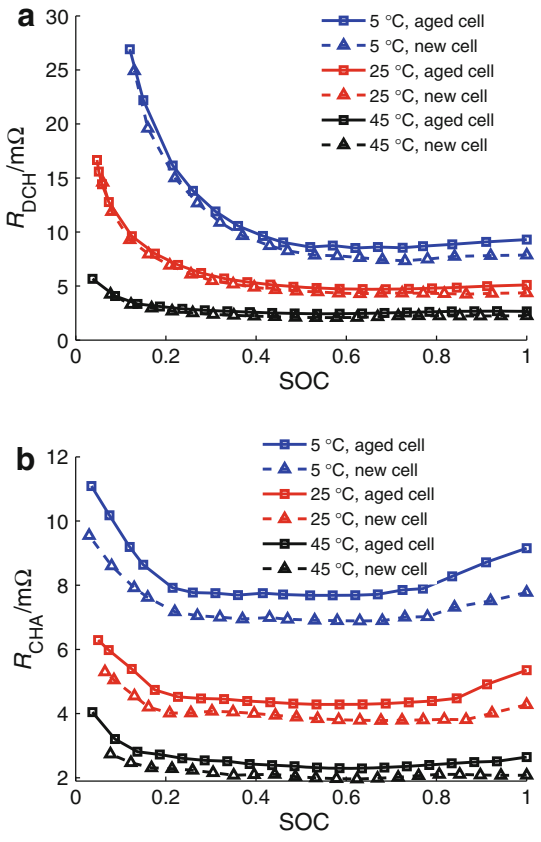

Fig. 1 Internal resistance under different temperatures and aging conditions. **a** Discharge internal resistance. **b** Charge internal resistance

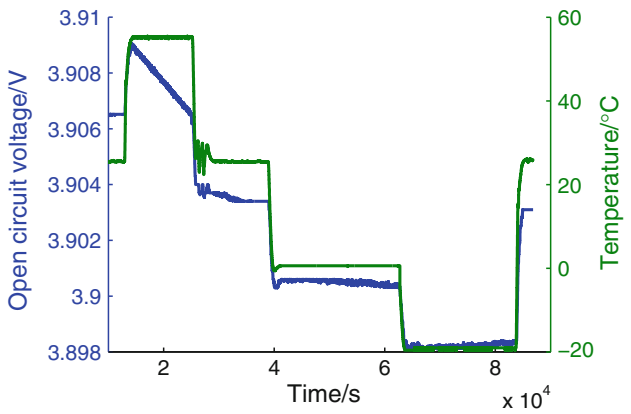

Fig. 2 Example of OCV variation during temperature cycle for aged cell at SOC 75 %

entropic heat coefficient (dU_{OCV}/dT) could be calculated by dividing the Faraday constant (96,485 C mol^{-1}). For out battery, a lumped dU_{OCV}/dT value is calculated by least-square method at each SOC point, and the result is compared with the reference in Fig. 4b. The general trend of dU_{OCV}/dT is identical between our battery and the cell in reference, but some difference exists. It is probably caused by the difference in electrode composition and manufacturing process between our test cell and the cell in reference.

Analysis of heat generation rate and ratio of Joule and reaction heat under different operating conditions

In order to estimate the battery temperature variation in real-world charging/discharging process, the generation rates of Joule heat and reaction heat should be analyzed under different operating conditions, including temperature, SOC, aging effect, and operating current. The ratio of Joule and reaction heat needs to be investigated as well, so as to analyze the heat generation source and offer advice for battery production modification. In this part, the heat generation rate and the heat generation ratio are discussed in detail based on the test data in the previous section, in consideration of the above-listed influencing factors.

Analysis of heat generation rate and ratio under fixed operating current

In order to explain the impact of operating conditions clearly, the influences of temperature and current are separately discussed. In this section, fixed operating current (1C discharge) is applied, and the heat generations under different temperatures (5, 25 and 45 °C) and different SOCs are analyzed for both the new and aged cells. The generation rates of Joule heat, reaction heat, and total heat at 5 °C are shown in Fig. 5a, and the results under 25 and 45 °C are provided in Fig. 5b, c. Figure 6 calculates the ratio of reaction heat and Joule heat under different temperatures and aging conditions. The values of average heat generation rate and the ratio of reaction and Joule heats are presented in Table 1. Comparing Fig. 5a–c, it is obvious that the total heat generation rate decreases significantly with increasing temperature, which is mainly contributed by the Joule heat reduction. The role of reaction heat in the total heat generation is consequently more important at higher temperature.

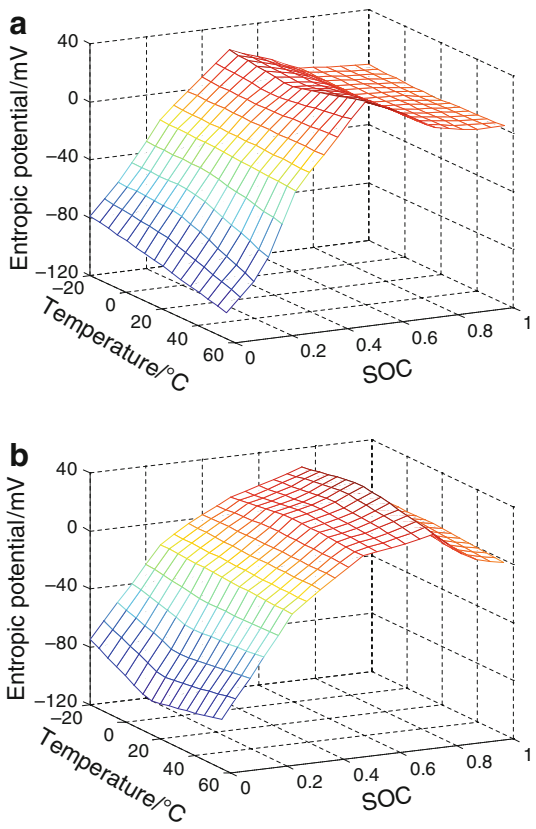

Fig. 3 Entropic potential under different SOC and temperature **a** new cell **b** aged cell

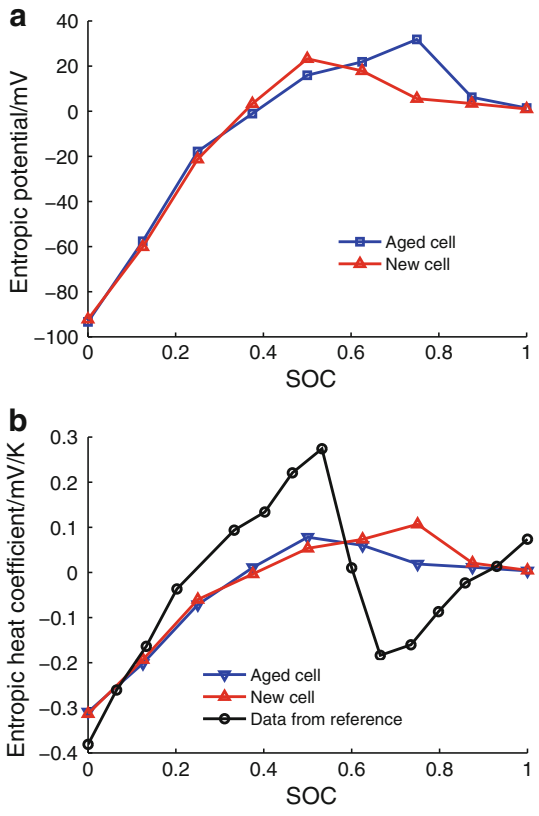

Fig. 4 Comparison of entropic parameters under different SOC **a** comparison of entropic potential for the new and aged cell at 25 °C **b** comparison of entropic heat coefficient between our LMO-G cell and the literature result

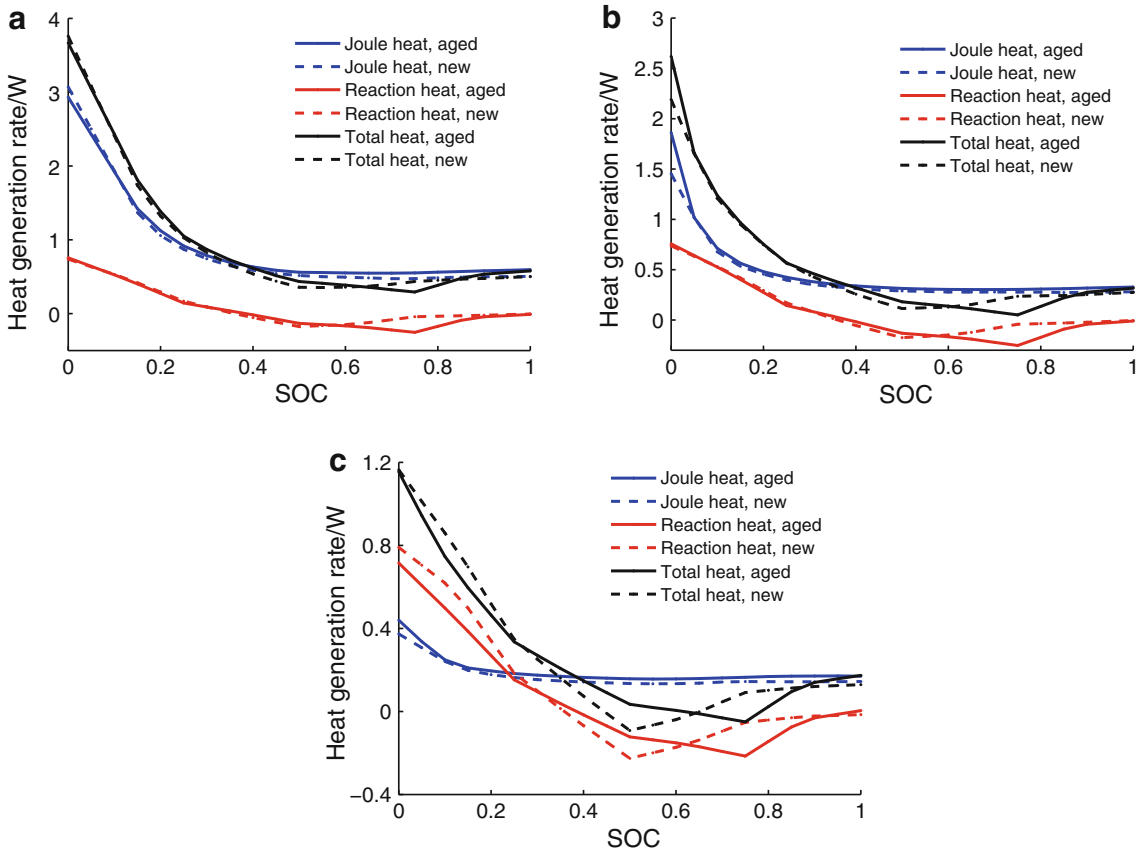

Fig. 5 Battery heat generation rate under different temperatures, SOCs, and aging conditions. **a** 5 °C, **b** 25 °C, and **c** 45 °C

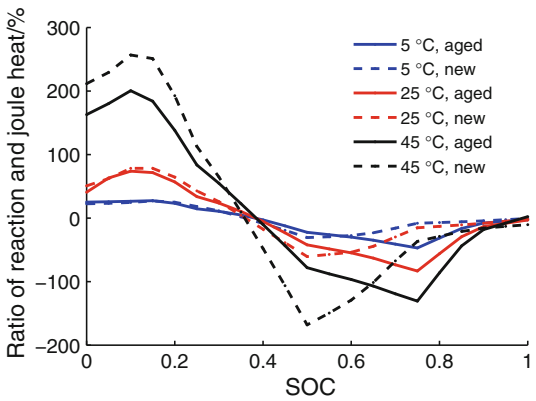

Fig. 6 Ratio of reaction heat and Joule heat under different temperatures, SOCs and aging conditions

Both the Joule and reaction heats are relatively large at low-SOC range. At high SOC, the Joule heat becomes smaller, while reaction heat is mostly negative, leading to a small or even negative total heat generation. Battery aging has little effect on the average heat generation rate under 1C discharge, since the discharge resistance growth is very limited during 300 charge–discharge cycles (shown in Fig. 1a). But the aging effect must be considered for some batteries with large resistance growth (for example the cells in [22]). In addition, the heat generation in SOC 65–85 % is quite different for the new and aged cell, which requires consideration especially under high-temperature conditions.

Table 1 Average heat generation rate and ratio of reaction and Joule heats under different temperatures and aging conditions (1C discharge)

	Avg. heat generation rate/W	Max. ratio of $\dot{Q}_{re}$ and $\dot{Q}_{jou}$/%	Min. ratio of $\dot{Q}_{re}$ and $\dot{Q}_{jou}$/%	Avg. ratio of $\dot{Q}_{re}$ and $\dot{Q}_{jou}$/%
5 °C aged	0.937	27.4	−47.0	4.7
5 °C new	0.917	27.0	−30.7	8.1
25 °C aged	0.487	73.9	−83.5	10.8
25 °C new	0.477	78.3	−60.7	18.8
45 °C aged	0.242	200.5	−130.7	28.2
45 °C new	0.248	256.6	−168.1	49.2

Analysis of heat generation rate and ratio under fixed ambient temperature

In this part, the heat generations under different discharge currents (1C discharge, 1C charge, 2C and 4C discharge)

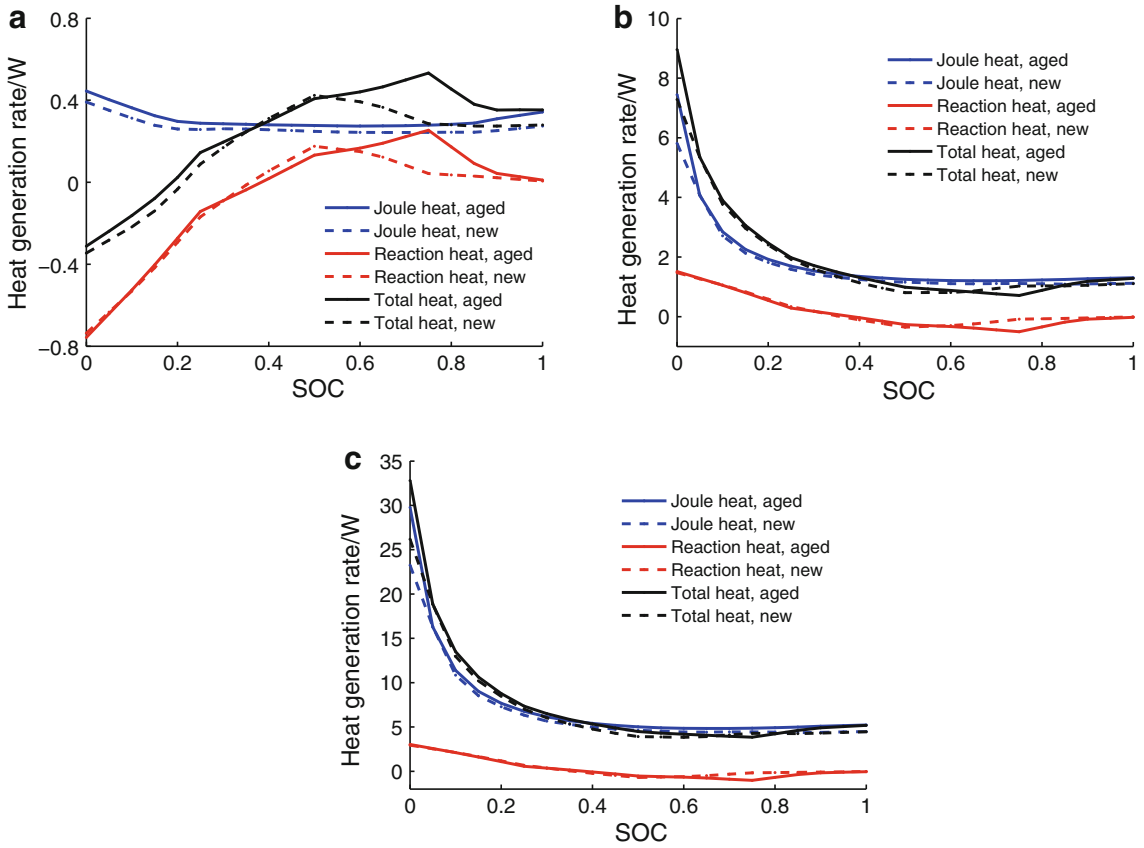

Fig. 7 Battery heat generation rate under different currents, SOCs, and aging conditions: **a** 1C charge, **b** 2C discharge, and **c** 4C discharge

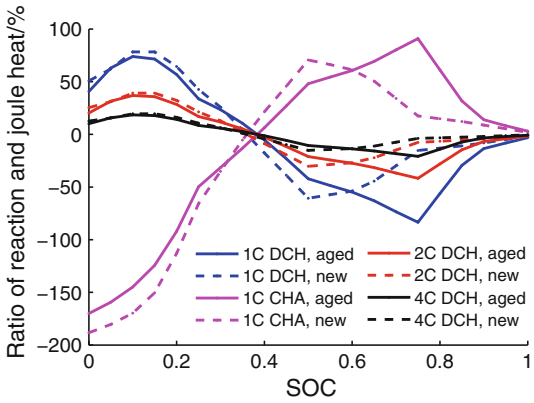

Fig. 8 Ratio of reaction heat and Joule heat under different currents, SOCs and aging conditions

and SOC are discussed for the new and aged cell, and all these analyses are under a fixed operating temperature (25 °C). The result for 1C discharge at 25 °C has already been presented in Figs. 5b and 7a–c, which provide the heat generation rate under 1C charge, 2C discharge, and 4C discharge separately. Figure 8 shows the ratio of reaction heat and Joule heat under different currents and aging conditions. The values of total heat generation rate and the ratio of reaction and Joule heat are listed in Table 2. In Fig. 8 and Table 2, "discharge" is abbreviated with "DCH" and "charge" with "CHA".

It can be seen that the total heat generation rate rises greatly with increasing discharge current, since Joule heat is quadratic dependent on current, and reaction heat is proportional dependent (shown in Eq. 2). This relationship can also explain why the reaction heat is less important at larger discharge current (10.8 % of $\dot{Q}_{\mathrm{jou}}$ at 1C, 5.4 % at 2C and 2.7 % at 4C, for aged cell, e.g.). The average heat under 1C charge is obviously smaller than 1C discharge, and two possible reasons are responsible. First, the charge resistance is smaller than discharge resistance (shown in Fig. 1), leading to decrease in Joule heat production. Second, the reaction heat is negative (−15.7 % of $\dot{Q}_{\mathrm{jou}}$ for aged cell, e.g.) upon charge and positive upon discharge (10.8 % of $\dot{Q}_{\mathrm{jou}}$, aged cell), which results in a heat-production gap between charge and discharge. The importance of reaction heat in charging process is, therefore, greater, which is shown clearly in Fig. 8 by comparing the magenta and blue curve. The charge Joule heat is quite constant at different SOCs, and the variation of total heat generation depends largely on the SOC influence on reaction heat (as in Fig. 6a).

As discharge current increases, the influence of battery aging also becomes greater. Listed in Table 2, the heat

Table 2 Average heat generation rate and ratio of reaction and Joule heat under different currents and aging conditions (25 °C)

	Avg. heat generation rate/W	Max. ratio of $\dot{Q}_{re}$ and $\dot{Q}_{jou}$/%	Min. ratio of $\dot{Q}_{re}$ and $\dot{Q}_{jou}$/%	Avg. ratio of $\dot{Q}_{re}$ and $\dot{Q}_{jou}$/%
1C DCH, aged	0.487	73.9	−83.5	10.8
1C DCH, new	0.477	78.3	−60.7	18.8
1C CHA, aged	0.255	90.9	−170.0	−15.7
1C CHA, new	0.189	70.6	−188.4	−28.5
2C DCH, aged	1.851	36.9	−41.7	5.4
2C DCH, new	1.756	39.1	−30.4	9.4
4C DCH, aged	7.216	18.5	−20.9	2.7
4C DCH, new	6.721	19.6	−15.2	4.7

generation deviation between aged and new cell under 1C discharge is 0.01 W, while the difference is 0.55 W under 4C discharge. Under 1C charge, the average heat of aged cell is 34.9 % larger than the new cell, while under 1C discharge the difference is only 2.1 %, meaning that aging effect is more crucial for heat generation in charging than in discharging. This phenomenon probably arises from the large charge resistance growth in cell degradation, as shown in Fig. 1b.

Experimental validation of heat generation analysis through temperature variation calculation

In previous parts, the heat generation under different operating conditions is analyzed in detail. In order to validate the heat generation results, battery temperature variation during charge/discharge should be estimated based on the heat generation calculation and battery heat transfer model. By comparing the calculated temperature change and the experimental results, the accuracy of our heat generation analysis can be verified.

Under low- and middle-current rate, the maximum temperature difference within a cell is limited [6], and the heat generating factors are assumed to change linearly with temperature [23]. As a result, a lumped thermal model with a "cell average temperature" can be used to calculate battery heat generation, which could provide accurate temperature estimation results in battery management system applications [24, 25]. And the simplicity of the lumped model makes it very suitable for online applications [24]. As a result, lumped thermal model is here implemented for temperature prediction during charge/discharge process. The temperature variation is calculated in Eq. 4, in with m is battery mass, c_p is heat capacity, T is current battery temperature and $\mathrm{d}T/\mathrm{d}t$ is the rate of temperature variation, $\dot{Q}$ is the heat generation rate, h is heat

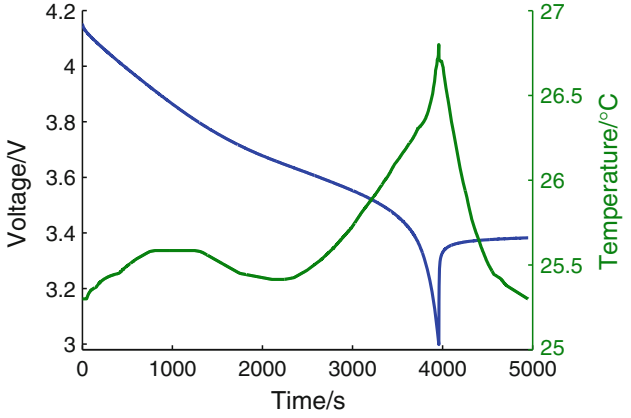

Fig. 9 Variation of battery voltage and temperature during discharge and rest period (1C discharge, environment temperature 25.2 °C)

convection coefficient, A is battery surface area, and T_{env} is the environment temperature. The first term on the right side represents the heat generation rate, and the second term is the heat dissipation rate. During our test in this part, the battery temperature variation is limited (<5 °C), which means the heat capacity c_p and heat convection coefficient h could be assumed as constant [9, 10, 26, 27]. Equation 4 can be written in another form in Eq. 5, in which k_1 (equals $1/mc_p$) represents the parameter for heat generation, and k_2 (equals hA/mc_p) represents the parameter for heat dissipation. Since the relevant battery parameters (h, A, m, and c_p) are all constant in our assumption, lumped k_1 and k_2 values could be identified by experimental results.

The voltage and temperature variation under 1C (8 A) discharge experiment (new cell, environment temperature 25.2 °C) are shown in Fig. 9. In "rest period" (the time period from the voltage ebb to the end), the discharge current as well as the heat generation rate is zero. As a result, the heat dissipation parameter k_2 can be identified through least square regression. Then, the heat generation parameter k_1 could be calculated with the temperature data in "discharge period" (the time period from the start to the voltage ebb) in Fig. 9, as shown in Eq. 6. t_1 and t_2 are the start and end times of discharge period, and the heat generation rate $\dot{Q}$ comes from the analysis results in the previous section. The heat capacity c_p and heat convection coefficient h could be derived from k_1 and k_2. Taking 1C discharge process for the new cell as an example, cell mass m is 0.295 kg, and the total area A is 0.037 m^3 (height 142 mm, width 115 mm, and thickness 0.0085 mm). A 500-s rest period was chosen for least square calculation, with k_2 0.0033 1/s and k_1 0.0036 K J^{-1}. Consequently, the heat transfer coefficient h is the 24.927 W m^{-2} K^{-1}, and the heat capacity c_p is 939.7 J kg^{-1} K^{-1} which is reasonable for battery under weak forced convection condition [9].

$$mc_p \frac{dT}{dt} = \dot{Q} - hA(T - T_{env}) \quad (4)$$

$$\frac{dT}{dt} = \frac{\dot{Q}}{mc_p} - \frac{hA}{mc_p}(T - T_{env}) = k_1\dot{Q} - k_2(T - T_{env}) \quad (5)$$

$$k_1 = \frac{T_{t_2} - T_{t_1} + k_2 \int_{t_1}^{t_2} (T - T_{env})dt}{\int_{t_1}^{t_2} \dot{Q}dt} \quad (6)$$

After determining k_1 and k_2, the temperature variation can be calculated based on the initial temperature T_0, environment temperature T_{env}, and heat generation rate. In case of real time application, the calculation is in discrete form, and the iteration process is presented in Eq. 7. T_{k-1} is the calculated temperature at time $k-1$, and Δt is the discrete step time, $\dot{Q}_k$ is the heat generation rate at time k, and $T_{env,k-1}$ is the environment temperature at time $k-1$. The SOC at each time point is calculated in advance, so the corresponded heat generation rate $\dot{Q}_k$ can be looked up in Fig. 5b. Figure 10a compares the calculated temperature profile and the measured temperature with a 1-s step time. The average temperature difference is 0.006 °C, and the maximum difference is 0.2 °C, validating the accuracy of temperature variation calculation. Consequently, the heat generation rate analysis is proved to be accurate under 1C discharge for the new cell.

$$T_k = T_{k-1} + \Delta t \cdot [k_1\dot{Q}_k - k_2(T_{k-1} - T_{env,k-1})] \quad (7)$$

In order to validate the temperature results considering battery aging, the same analyzing procedures are executed for the aged cell (1C discharge, environment temperature 25.3 °C), and the heat generation information also comes from Fig. 5b. Analyzed and experimental results are compared in Fig. 10b, in which the average temperature deviation is 0.011 °C, and the maximum error is 0.15 °C. During 1C discharge, temperature decrease is observed for both the new and aged cells, but the decrease comes earlier for the aged cell, due to the reaction heat difference. Consequently, the aging effect should be considered to get a precise prediction of temperature variation.

Figure 10c, d presents the temperature variation under 2C (16A) and 4C (32A) discharge for the new cell. The average temperature differences between calculated and measured value are separately 0.024 and 0.107 °C, and the maximum errors are 0.25 and 0.59 °C. The calculation error is acceptable but enlarged comparing to 1C discharge, probably because of the fluctuation of environment temperature during large current experiment.

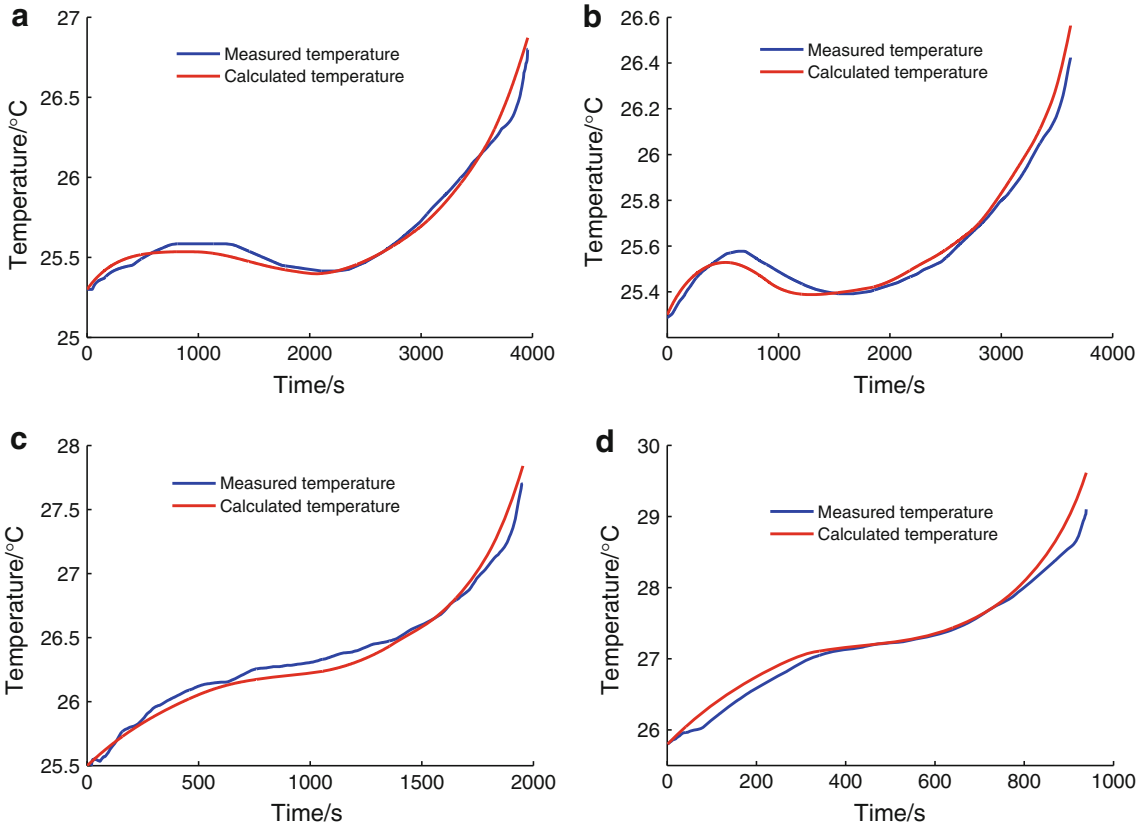

Fig. 10 Comparison of the calculated and measured temperature variation under different operating currents and aging conditions: **a** new cell, 1C discharge; **b** aged cell, 1C discharge; **c** new cell, 2C discharge; and **d** new cell, 4C discharge

Conclusions

In order to predict the influence of battery temperature variation on EV performance, heat generation during charge and discharge should be analyzed in detail. Joule heat and reaction heat are the main heat sources, which depend largely on the operating conditions, including environment temperature, aging effect, SOC, and charge/discharge current.

In this article, we execute a series of experiments to determine the heat generation parameters. The Joule heat parameter (internal resistance) is calibrated under different temperatures, SOC, and degradation conditions, and the reaction heat parameter (effective entropic potential) is calculated by measuring the OCV at different SOC under a wide temperature range. It is concluded that the Joule heat increases at lower temperature and as the cell ages, and the aging effect is more significant for charging process than discharging. In contrast, there is little variation for reaction heat generation in aging process in most of the SOC range. Battery SOC also influences the Joule heat and reaction heat generation rates. A larger operating current leads to greater Joule and reaction heat production, and causes the increase of Joule heat percentage in total heat generation.

Based on heat generation analysis, a lumped thermal model is implemented to calculate battery temperature variation in charge/discharge process. The calculated temperature corresponds well with experimental results under different currents and aging conditions, proving the accuracy of heat generation analysis. Consequently, if the current input is known, this method can be performed to predict the future temperature variation. It is also promising to apply the method on EV battery management system owing to its simplicity.

Acknowledgements This research is funded by the MOST (Ministry of Science and Technology) of China (Grant No. 2011AA11A227 and 2010DFA72760) and the MOE (Ministry of Education) of China (Grant No. 2012DFA81190).

References

1. Zhang J, Lee J. A review on prognostics and health monitoring of Li-ion battery. J Power Sources. 2011;196:6007–14.
2. Zhao XW, Zhang GY, Yang L, et al. A new charging mode of Li-ion batteries with LiFePO4/C composites under low temperature. J Therm Anal Calorim. 2011;104:561–7.
3. Bhide S, Shim T. Novel predictive electric Li-ion battery model incorporating thermal and rate factor effects. IEEE Trans Veh Technol. 2011;60:819–29.
4. Lu TY, Chiang CC, Wu SH, et al. Thermal hazard evaluations of 18650 lithium-ion batteries by an adiabatic calorimeter. J Therm Anal Calorim. 2013; doi: 10.1007/s10973-013-3137-9.
5. Lu L, Han X, Li J, et al. A review on the key issues for lithium-ion battery management in electric vehicles. J Power Sources. 2013;226:272–88.
6. Yang K, An JJ, Chen S. Temperature characterization analysis of LiFePO4/C power battery during charging and discharging. J Therm Anal Calorim. 2010;99:515–21.
7. Fang K, Chen S, Mu D, et al. The heat generation rate of nickel-metal hydride battery during charging/discharging. J Therm Anal Calorim. 2013;112:977–81.
8. Bandhauer TM, Garimella S, Fuller TF. A critical review of thermal issues in lithium-ion batteries. J Electrochem Soc. 2011; 158:R1–25.
9. Chen SC, Wan CC, Wang YY. Thermal analysis of lithium-ion batteries. J Power Sources. 2005;140:111–24.
10. Wu W, Xiao X, Huang X. The effect of battery design parameters on heat generation and utilization in a Li-ion cell. Electrochim Acta. 2012;83:227–40.
11. Forgez C, Do DV, Friedrich G, et al. Thermal modeling of a cylindrical $LiFePO_4$/graphite lithium-ion battery. J Power Sources. 2010;195:2961–8.
12. Thomas KE, Newman J. Thermal modeling of porous insertion electrodes. J Electrochem Soc. 2003;150:A176–92.
13. Andrea D, Meiler M, Steiner K, et al. Characterization of high-power lithium-ion batteries by electrochemical impedance spectroscopy. I. Experimental investigation. J Power Sources. 2011; 196:5334–41.
14. Ecker M, Gerschler JB, Vogel J, et al. Development of a lifetime prediction model for lithium-ion batteries based on extended accelerated aging test data. J Power Sources. 2012;215:248–57.
15. Viswanathan VV, Choi D, Wang D, et al. Effect of entropy change of lithium intercalation in cathodes and anodes on Li-ion battery thermal management. J Power Sources. 2010;195:3720–9.
16. Thomas KE, Bogatu C, Newman J. Measurement of the entropy of reaction as a function of state of charge in doped and undoped lithium manganese oxide. J Electrochem Soc. 2001;148:A570–5.
17. Matthe R, Turner L, Mettlach H. VOLTEC battery system for electric vehicle with extended range. SAE Int J Engines. 2011;4: 1944–62.
18. Battery Test Manual for Plug-In Hybrid Electric Vehicles. Idaho National Laboratory. 2010. http://www.inl.gov/technicalpublications/Documents/4655291.pdf. Accessed 10 May 2013.
19. Remmlinger J, Buchholz M, Meiler M, et al. State-of-health monitoring of lithium-ion batteries in electric vehicles by on-board internal resistance estimation. J Power Sources. 2011;196: 5357–63.
20. Thomas KE, Newman J. Heats of mixing and of entropy in porous insertion electrodes. J Power Sources. 2003;119–121:844–9.
21. Dubarry M, Truchot C, Liaw BY. Synthesize battery degradation modes via a diagnostic and prognostic model. J Power Sources. 2012;219:204–16.
22. Belt J, Utgikar V, Bloom I. Calendar and PHEV cycle life aging of high-energy, lithium-ion cells containing blended spinel and layered-oxide cathodes. J Power Sources. 2001;196:10213–21.
23. Zheng Y, Han X, Lu L, et al. Lithium ion battery pack power fade fault identification based on Shannon entropy in electric vehicles. J Power Sources. 2013;223:136–46.
24. Chiang CJ, Yang JL, Cheng WC. Temperature and state-of-charge estimation in ultracapacitors based on extended Kalman filter. J Power Sources. 2013;234:234–43.
25. Brown D, Landers RG. Control oriented thermal modeling of lithium ion batteries from a first principle model via model reduction by the global Arnoldi algorithm. J Electrochem Soc. 2012;159:A2043–52.
26. Onda K, Ohshima T, Nakayama M, et al. Thermal behavior of small lithium-ion battery during rapid charge and discharge cycles. J Power Sources. 2006;158:535–42.
27. Ye Y, Shi Y, Cai N, et al. Electro-thermal modeling and experimental validation for lithium ion battery. J Power Sources. 2012;199:227–38.